

Transient Thermal Analysis of Space Rectangular Thin-Walled Structures by Carrera Unified Formulation

Original

Transient Thermal Analysis of Space Rectangular Thin-Walled Structures by Carrera Unified Formulation / Zhou, X., Masia, R., Zhu, R., Pagani, A., Carrera, E., Chen, W.. - In: AIAA JOURNAL. - ISSN 0001-1452. - 62:6(2024), pp. 2313-2320. [10.2514/1.j063671]

Availability:

This version is available at: 11583/2989575 since: 2024-06-17T09:04:27Z

Publisher:

AMER INST AERONAUTICS ASTRONAUTICS

Published

DOI:10.2514/1.j063671

Terms of use:

This article is made available under terms and conditions as specified in the corresponding bibliographic description in the repository

Publisher copyright

(Article begins on next page)



Transient thermal analysis of space rectangular thin-walled structures by CUF

Journal:	<i>AIAA Journal</i>
Manuscript ID	2023-10-J063671.R1
Manuscript Type:	Regular Article
Date Submitted by the Author:	n/a
Complete List of Authors:	Zhou, Xiaoliang; Zhejiang University Masia, Rebecca; Politecnico di Torino, Department of Mechanical and Aerospace Engineering Zhu, Rujiang; China Academy of Space Technology Pagani, Alfonso; Politecnico di Torino, Department of Mechanical and Aerospace Engineering Carrera, Erasmo; Politecnico di Torino, Department of Mechanical and Aerospace Engineering Chen, Weiqiu; Zhejiang University
Subject Index Category:	90400 Computational Heat Transfer < 90000 THERMOPHYSICS AND HEAT TRANSFER, 90000 THERMOPHYSICS AND HEAT TRANSFER
Select ONE Subject Index for the Table of Contents. This is where your paper will show up in the Table of Contents:	90000 THERMOPHYSICS AND HEAT TRANSFER

SCHOLARONE™
Manuscripts

Transient thermal analysis of space rectangular thin-walled structures by CUF

Xiaoliang Zhou*

China Academy of Space Technology Hangzhou Institute, Hangzhou, 310024, China

Zhejiang University, Hangzhou, 310027, China

Rebecca Masia†

Politecnico di Torino, Turin, 10129, Italy

Rujian Zhu‡

China Academy of Space Technology Hangzhou Institute, Hangzhou, 310024, China

Alfonso Pagani§ and Erasmo Carrera**
Politecnico di Torino, Turin, 10129, Italy

and

Weiqliu Chen††

Zhejiang University, Hangzhou, 310027, China

The accurate prediction of transient thermal fields of space structures is of paramount significance for the analysis of geometrical stability and thermal management systems. This paper proposes a novel method to solve the transient thermal field of the thin-walled cross-section of beams in outer space. High-order beam elements are derived by means of the Carrera Unified Formulation (CUF), where the longitudinal direction of the beam is discretized by one-dimensional two-nodes and four-nodes elements, whereas arbitrary high order expansion functions are used for the description of the temperature expansion within the cross-section. The governing differential equations of transient temperature field are derived according to the transient thermal conduction theory and the weighted residual method. The solution of the initial value problem for ordinary differential equations is obtained through the application of the Adams-Bashforth method, leading to the

* Postdoctoral, Department of Engineering Mechanics, Zhejiang University.

† PhD student, Department of Mechanical and Aerospace Engineering.

‡ PhD.

§ Associate Professor, Department of Mechanical and Aerospace Engineering, corresponding author, alfonso.pagani@polito.it

** Professor, Department of Mechanical and Aerospace Engineering.

†† Professor, Shenzhen Research Institute, Department of Engineering Mechanics; also Shenzhen Research Institute of Zhejiang University, 518057 Shenzhen, People's Republic of China.

1
2
3 **determination of the transient thermal field. In order to demonstrate the accuracy of the**
4 **temperature results, a convergence analysis is conducted. Finally, temperature distributions**
5 **within the cross- section and along the longitudinal direction of the model are discussed to**
6 **show the effects of several factors including material properties, angle of solar radiation,**
7 **shadows induced by the shelter of other components.**
8
9
10
11
12
13
14

15 **Nomenclature**

16	A	=	domain of integration within the cross section
17	a	=	side length of the cross section
18	C^{rsij}	=	fundamental nucleus of specific heat matrix
19	C_p	=	specific heat
20	dt	=	time step
21	F_r, F_s	=	expansion functions within the cross section
22	K^{rsij}	=	fundamental nucleus of heat conduction coefficient matrix
23	k_x	=	thermal conductivity in the x direction
24	k_y	=	thermal conductivity in the y direction
25	k_z	=	thermal conductivity in the z direction
26	L	=	the length of the thin-walled structure
27	L_s	=	the length of the shadow area
28	N_i, N_j	=	the shape functions of beam element
29	N_n	=	the number of beam element nodes
30	M	=	the number of terms in the expansion within the cross-section
31	Q^{sj}	=	fundamental nucleus of the solar radiation heating matrix
32	q	=	the heat flux of solar radiation
33	R^{sj}	=	fundamental nucleus of the radiation dissipation matrix
34	T	=	temperature of the node
35	\mathbf{T}	=	temperature fields of the thin-walled structure
36	T_{sur}	=	temperature of the outer space

1		
2		
3	t_s	= thickness of thin-walled beam
4		
5	ρ	= mass density
6		
7	ε	= emissivity of the external boundaries
8		
9	σ	= Stefan-Bolzman constant
10		
11	α_s	= absorptivity of boundaries
12		
13	Γ_1	= the solar radiation boundaries
14		
15	Γ_2	= the radiation dissipation boundaries
16		

17 I. Introduction

18
19
20 **T**HE structural components of space aircraft, such as beams and plates, are routinely exposed to extreme low and
21 high temperatures during their in-orbit operations [1-3]. Due to the need of the structural components to be
22 deployable and lightweight, thin-wall structures are usually used in the design [4-6]. Thermally induced vibrations
23 may be easily triggered when lightweight and flexible structures encounter rapid elevated temperatures. On the other
24 hand, undesirable thermal buckling which could result in a reduction of load-bearing capacity or even failure of
25 structure, may occur when the thermal stress reaches critical values. The failure of Hubble Space Telescope [7]
26 generated by thermally induced vibration and the thermal buckling of its solar array, serves as a notable example.
27 Therefore, conducting transient thermal analysis of thin-walled structures holds great significance for the thermo-
28 mechanical coupling analyses of thin-walled components of space aircraft [8].
29
30
31
32
33
34
35
36

37 Obtaining the analytical solution of transient thermal analysis is challenging due to the existence of the radiation
38 dissipation quartic item. The 3D finite element method, using block or shell elements, is suitable for analyzing space
39 thin-walled structures while taking into account the quartic item and time-dependent heating sources [9-11].
40 Nevertheless, a large number of elements and, thus, degrees of freedom can significantly affect the computational
41 efficiency. When the heating source of solar radiation is independent of the axis coordinate, it becomes possible to
42 disregard the temperature differences along the axis direction. This simplification enables the 3D thermal analysis to
43 be treated as a two-dimensional (2D) problem [12]. The 2D Finite Element Method (FEM) model has obvious
44 advantages on computational efficiency compared with 3D analyses, nevertheless they do not provide through-the-
45 thickness temperature distribution, which can be of certain importance in the design of thermal management systems
46 or measurement tools.
47
48
49
50
51
52
53
54
55
56
57
58
59
60

1
2
3 Despite numerical methods such as FEM, many researchers have also concentrated on the analytical approaches.
4
5 In order to analytically predict the thermal-structural response of a spinning spacecraft boom with hollow circular
6
7 cross-section, several assumptions, including constant and uniform solar heat flux and no thermal conduction along
8
9 the axis direction, constant temperature across the thickness of the tube for the determination of boom's temperature
10
11 distribution have been drawn by the Thorton group [13,14]. Then, they decompose the temperature into an average
12
13 term and perturbation terms to enable solving the non-linear item T4. On the basis of Thorton group's research,
14
15 Ding and Xue [15] proposed a Fourier finite element method which adopts beam elements in the axis direction and
16
17 Fourier series for the temperature gradient in the circumferential direction. However, the Fourier finite element is
18
19 suitable for circular tube, but may not be applicable for rectangular tubes. Therefore, to solve this problem, Xue and
20
21 Ding [16] have applied the Taylor polynomials as shape functions of temperature along the rectangular cross-
22
23 section. However, they have only considered linear polynomials, which result in linear distribution of the
24
25 temperature along the edges of the rectangular cross-section. The Fourier element method has been applied in
26
27 several nearest investigations that concentrate on thermal-structural analyses of thin-walled beams [17-20].

28 Although the Fourier element method offers several advantages when dealing with transient thermal analyses of
29
30 thin-walled beams, it is crucial to acknowledge that several assumptions adopted in the method can lead to
31
32 discrepancies when compared to the 3D FEM results. These assumptions include the absence of temperature
33
34 gradient through the thickness, linear distribution of the temperature along the edges of rectangular cross-sections.
35
36 Conversely, 2D analyses may be inapplicable when dealing with scenarios where the heating source of solar
37
38 radiation is not constant along the beam direction. Therefore, to establish a balance between the result accuracy and
39
40 the computational efficiency in 3D thermal analysis, the Carrera Unified Formulation (CUF) [21] is adopted to solve
41
42 transient thermal conduction issues. One of the advantages of the CUF theory is that the computational efficiency is
43
44 significantly improved by making use of arbitrary expansion functions, instead of 3D shape functions, for expressing
45
46 the variables over the cross-section of beams or width of plates. Many engineering problems have been investigated
47
48 in the CUF framework, such as aerospace constructions [22, 23], composite structures [24-26], civil engineering
49
50 applications [27, 28], multi-field analyses [29, 30] and free vibration [31, 32]. However, the transient thermal
51
52 analysis of space thin-walled beams using the CUF theory has not been undertaken this far.

53 Therefore, the present research proposes transient thermal analyses based on the CUF theory to introduce a novel
54
55 approach aimed at enhancing high-level of computational efficiency when dealing with the thin-walled beams in
56
57
58
59
60

outer space. The article is organized as follows. The transient thermal analysis equations based on the CUF theory are derived in Section 2. The Lagrange Expansion (LE) model is introduced in Section 3. Section 4 presents numerical instances including convergence analyses on beam elements, the influence of the solar radiation angle and the shadow area on the temperature field. The conclusions are summarized in Section 5.

II. Mathematical framework

A beam model with a thin-walled cross-section under the heating load from solar radiation is shown in Figure 1. Due to small the size of the cross-section, only the thermal emission by radiation dissipation of external surfaces is considered while the energy emission of internal surfaces is neglected. All the thermal properties of the material are assumed to be independent of the temperature.

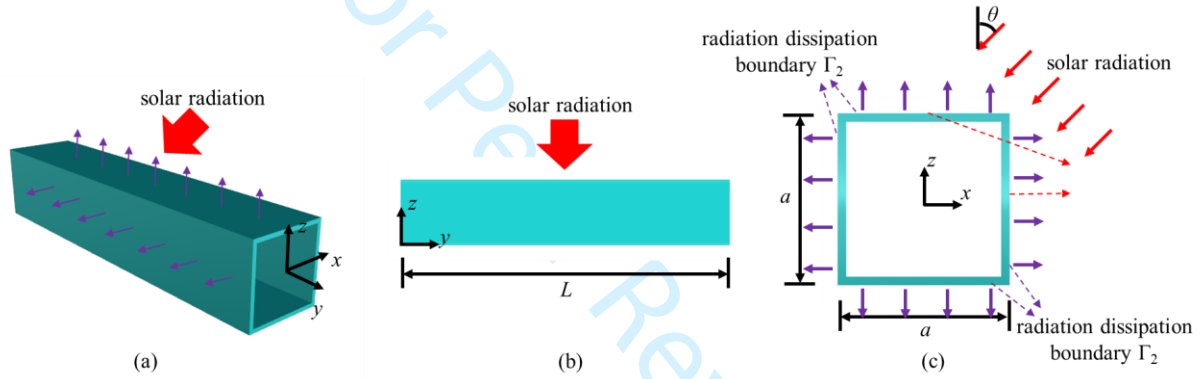


Fig. 1 Schematic diagram of a space thin-walled beam with square cross-section under the heating load of solar radiation.

According to the transient heat conduction theory, the governing partial differential equation of temperature field can be rewritten as [33]:

$$\rho C_p \frac{\partial T}{\partial t} - \frac{\partial}{\partial x} \left(k_x \frac{\partial T}{\partial x} \right) - \frac{\partial}{\partial y} \left(k_y \frac{\partial T}{\partial y} \right) - \frac{\partial}{\partial z} \left(k_z \frac{\partial T}{\partial z} \right) = 0 \quad (1)$$

where ρ is density, C_p is specific heat, t is the time, k_x , k_y and k_z are the thermal conductivities along the three directions, respectively. The following two boundary conditions shall be satisfied,

$$k_x \frac{\partial T}{\partial x} n_x + k_y \frac{\partial T}{\partial y} n_y + k_z \frac{\partial T}{\partial z} n_z = \alpha_s q(t) \quad \text{on the } \Gamma_1 \text{ boundary} \quad (2)$$

$$k_x \frac{\partial T}{\partial x} n_x + k_y \frac{\partial T}{\partial y} n_y + k_z \frac{\partial T}{\partial z} n_z = \varepsilon \sigma (T^4 - T_{sur}^4) \quad \text{on the } \Gamma_2 \text{ boundary} \quad (3)$$

where α_s is the absorptivity of the solar radiation boundary Γ_1 , $q(t)$ is the heat flux, which depends on the angle of the solar radiation, and ε is the emissivity of the external boundary Γ_2 , σ is the Stefan-Boltzman constant.

Using the weight residual method and adopting δT as weight function, the equation (1-3) can be transferred into integral form as follows,

$$\int_{\Omega} \left[\delta T \left(\rho C_p \frac{\partial T}{\partial t} \right) + \frac{\partial \delta T}{\partial x} \left(k_x \frac{\partial T}{\partial x} \right) + \frac{\partial \delta T}{\partial y} \left(k_y \frac{\partial T}{\partial y} \right) + \frac{\partial \delta T}{\partial z} \left(k_z \frac{\partial T}{\partial z} \right) \right] d\Omega - \int_{\Gamma_1} \delta T \alpha_s q(t) d\Gamma - \int_{\Gamma_2} \delta T \varepsilon \sigma (T^4 - T_{sur}^4) d\Gamma = 0 \quad (4)$$

Based on the CUF theory [21, 33], the variables field can be rewritten in a generalized form by adopting arbitrary expansion functions (such as the Lagrange and Taylor expansions). Therefore, the temperature field can be expanded as

$$T(x, y, z, t) = T_{\tau i}(t) F_{\tau}(x, z) N_i(y) \quad i = 1, \dots, N_n \quad \tau = 1, \dots, M \quad (5)$$

where N_n is the number of beam element nodes, M stands for the number of terms in the expansion within the cross-section. F_{τ} are the expansion functions in coordinates x and z , N_i are the shape functions of beam element. The summing convention with repeated indexes τ and i is assumed. The choice of functions F_{τ} , N_i and order M , N_n directly affects the accuracy of temperature result. The following form can be obtained by substituting Eq. (5) into Eq. (4):

$$\begin{aligned} & \rho C_p \iint_A F_{\tau} F_s dx dz \int_L N_i N_j dy \frac{dT_{\tau i}}{dt} + \iint_A k_x \frac{\partial F_{\tau}}{\partial x} \frac{\partial F_s}{\partial x} dx dz \int_L N_i N_j dy T_{\tau i} \\ & + \iint_A k_y F_{\tau} F_s dx dz \int_L \frac{\partial N_i}{\partial y} \frac{\partial N_j}{\partial y} dy T_{\tau i} + \iint_A k_z \frac{\partial F_{\tau}}{\partial z} \frac{\partial F_s}{\partial z} dx dz \int_L N_i N_j dy T_{\tau i} \\ & - \int_{\Gamma_1} \alpha_s q(t) F_s N_j d\Gamma + \int_{\Gamma_2} F_s N_j \varepsilon \sigma \left[(F_{\tau} T_{\tau i} N_i)^4 - T_{sur}^4 \right] d\Gamma = 0 \end{aligned} \quad (6)$$

The Eq. (6) can be written as a compact form:

$$\mathbf{C}^{\tau s i j} \dot{\mathbf{T}} + \mathbf{K}^{\tau s i j} \mathbf{T} - \mathbf{Q}^{s j} - \mathbf{R}^{s j} (\mathbf{T}^4) = \mathbf{0} \quad (7)$$

The Fundamental Nuclei (FN) $\mathbf{C}^{\tau s i j}$, $\mathbf{K}^{\tau s i j}$, $\mathbf{Q}^{s j}$, $\mathbf{R}^{s j}$ of Eq. (7) can be expressed as

$$\mathbf{C}^{\tau s i j} = \rho C_p \iint_A F_s F_{\tau} dx dz \int_L N_i N_j dy \quad (8)$$

$$\mathbf{K}^{\tau s i j} = k_x \iint_A \frac{\partial F_s}{\partial x} \frac{\partial F_{\tau}}{\partial x} dx dz \int_L N_i N_j dy + k_y \iint_A F_s F_{\tau} dx dz \int_L \frac{\partial N_i}{\partial y} \frac{\partial N_j}{\partial y} dy + k_z \iint_A \frac{\partial F_s}{\partial z} \frac{\partial F_{\tau}}{\partial z} dx dz \int_L N_i N_j dy \quad (9)$$

$$\mathbf{Q}^{sj} = \alpha_s \int_{\Gamma_1} F_s N_j q(t) d\Gamma \quad (10)$$

$$\mathbf{R}^{sj} = \varepsilon \sigma \int_{\Gamma_2} F_s N_j \left[\left(\sum_{\tau=1}^M \sum_{i=1}^{N_n} F_\tau N_i T_{\tau i} \right)^4 - T_{sur}^4 \right] d\Gamma \quad (11)$$

where $\tau, s=1, \dots, N_n, i, j=1, \dots, M$, the A denotes the integral domain of the cross-section, L denotes the integral domain along the longitudinal direction, T_{sur} is the temperature of the surroundings in outer space.

In the domain of CUF, the FNs are the basic building blocks for the development of arbitrary order computational order. They are 3x3 matrices that can be expanded against the indexes (i, τ) on the variables and (j, s) on the variations and they are independent of the theory approximation order F_τ and shape functions N_i . Interested readers are referred to as Carrera et al [21] for more details about the use of CUF-based finite elements.

III. CUF-based Lagrange Expansion (LE) models

In this paper, Lagrange polynomials are considered as F_τ functions for the description of the cross-section of the beam. In detail, four-node bilinear and nine-node quadratic elements are used on the domain of thin-walled cross-section. In this manner, temperature field within the cross-section is expanded as a series of Lagrange expansions whose detail expressions can be found in the literature [21, 34]. Details about the use of LE models in the context of CUF theory are also included for interested readers.

To effectively calculate the FNs in Eq. (8), the Gauss numerical integration method with six integration points is employed for solving the problem. Once all the FN have been obtained, the results for temperature fields are computed by solving the initial value problem of a series of nonlinear ordinary differential equations (ODEs) with quartic term in the time domain. There exist several approaches suitable for the initial problem, such as Euler method, modified Euler method, Runge-Kutta method, Adams-Bashforth method and many others. Here, the Adams-Bashforth method, a typical linear multi-step method, is adopted for the calculation of the ODEs, out of consideration of computational precision, convergence and computational speed.

IV. Numerical results

A. Convergence analysis and assessment

In order to assess the capability enhancement of the present CUF-based analysis, the transient temperature fields of thin-walled beams under solar radiation heating are addressed. Four different types of LE discretizations are adopted to reach the solution convergence for ensuring a fair comparison in terms of computational costs and precision. The features of the four LE discretizations are illustrated in Figure 2. As shown in Fig. 2, the first discretization in Fig. 2 (a) contains 20 linear elements (L4) and 40 nodes, the second (b) contains 36 linear elements (L4) and 72 nodes, the third (c) contains 8 quadratic elements (L9) and 48 nodes, the fourth (d) contains 12 quadratic elements (L9) and 72 nodes. Along the axial direction, linear and cubic beam element (B2 and B4) are employed to discretize the structure. In order to validate the accuracy of the present results, a finite element method model with linear/quadratic hexahedron elements is established in the software COMSOL Multiphysics to calculate the temperature fields simultaneously. The material properties considered in the numerical examples are shown in Table 1, where the a is the size of hollow square cross-section, t_s is the thickness of thin-walled beam, k is the thermal conductivity in the three directions, C_p is the specific heat, ρ is mass density, ε is the emissivity of the external boundaries, σ is the Stefan-Bolzman constant, α_s is the absorptivity, Q_s is the heat flux of solar radiation. The initial temperature of the whole area is settled to be 293.15K.

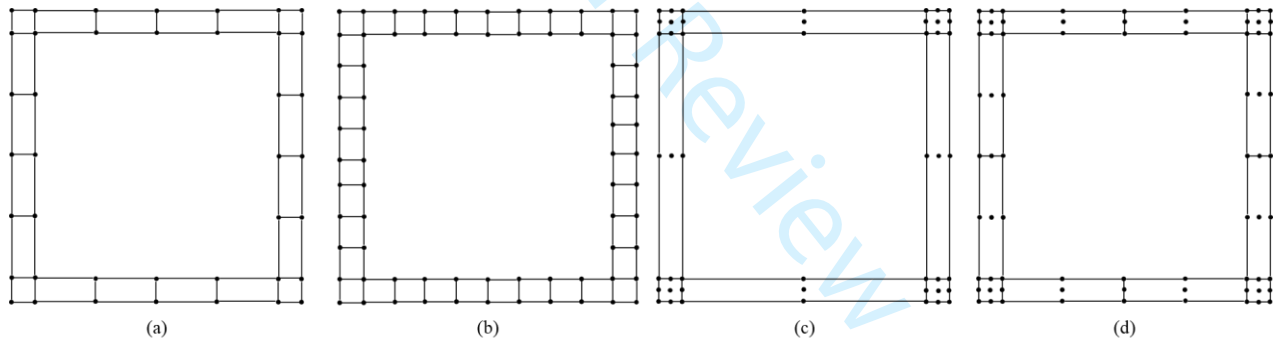


Fig. 2 Four types of closed thin-walled square cross-section discretizations, (a) 20 L4; (b) 36 L4; (c) 8 L9; (d) 12L9.

Table 1 Size and material properties of the thin-walled beam structure.

$a(\text{mm})$	$t_s(\text{mm})$	$k(\text{W/mK})$	$C_p(\text{J/kgK})$	$\rho(\text{kg/m}^3)$	ε	σ	α_s	$q(\text{W/m}^2)$
100	2.4	16.6	502	7010	0.13	5.67×10^{-8}	1.0	1350

Table 2 Temperatures at different points computed with different Lagrange expansion models when $t=3000\text{s}$.

	DOFs	point 1 (K)	point 2 (K)	point 3 (K)	point 4 (K)
FEM (linear hexahedron)	99384	342.5516	412.6838	439.0343	334.4747

elements)					
FEM (quadratic hexahedron elements)	200080	342.5050	412.7203	439.1479	334.4052
20L4-3B2	160	339.7931	408.4572	434.2495	332.0307
20L4-1B4	160	339.7932	408.4573	434.2495	332.0307
36L4-3B2	288	337.2141	405.4259	431.1315	329.5200
8L9-3B2	192	342.5632	411.9415	437.6518	334.7606
12L9-3B2	288	342.3198	411.7718	437.8168	334.3996

The temperatures at $t=3000s$ of four points obtained from different LE models and FEM analyses are shown in Table 2. The coordinates of the four points are $x_1=-50mm$, $z_1=-50mm$, $x_2=50mm$, $z_2=50mm$, $x_3=0mm$, $z_3=50mm$, $x_4=0mm$, $z_4=-50mm$, respectively. It is clear that, the accuracies of the two L9 models are significantly superior to L4 models. On the other hand, the results for B4 and B2 models do not exhibit relevant differences when dealing with the circumstance of constant heat flux along the axis direction. Furthermore, Figure 3 and Figure 4 illustrate the comparisons between the four types of LE results and FEM simulation. A similar conclusion can also be drawn from Figure 3 and 4, indicated that the LE model provides more accurate result for both the time history distribution and the spatial coordinate distribution.

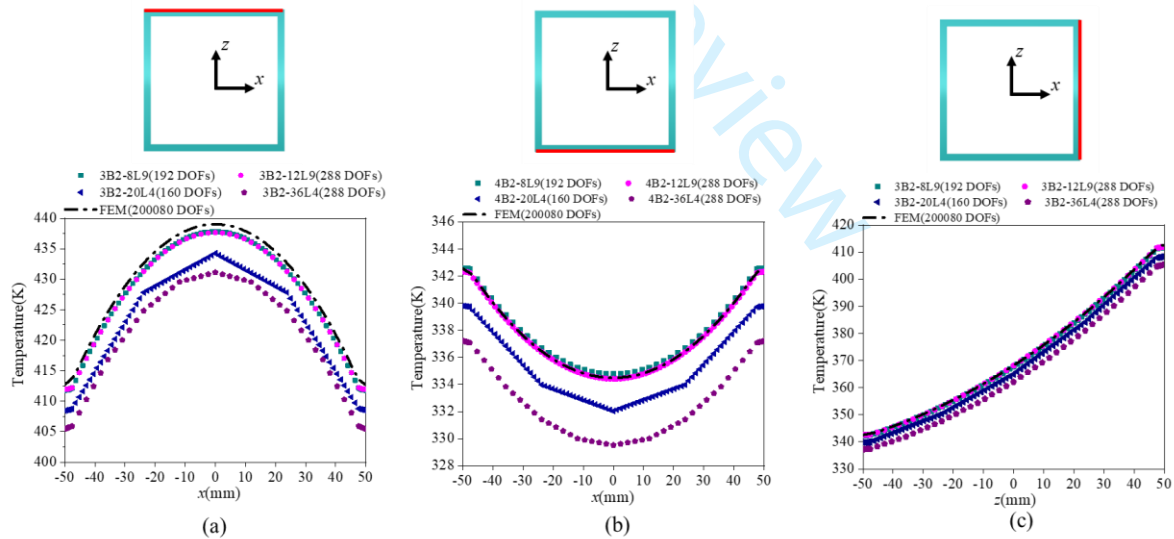


Fig. 3 (a) Temperature distribution along x -direction of the top edge; (b) temperature distribution along x -direction of the bottom edge; (c) temperature distribution along z -direction of the right edge.

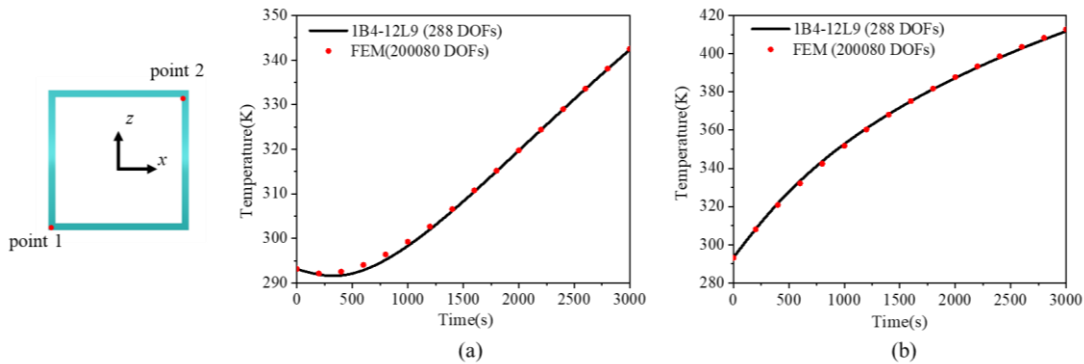


Fig. 3 Time history distributions of temperature of two points with coordinate of $x=-50\text{mm}$, $z=-50\text{mm}$ and $x=50\text{mm}$, $z=50\text{mm}$.

B. Temperature distributions of thin-walled beam under longitudinal constant heating sources

Figure 5 depicts the temperature distribution of the cross-section at the time intervals $t=1000\text{s}$, 2000s and 3000s . With the solar heat flux applied perpendicularly to the top surface, the highest temperature is registered in middle area of top surface and the lowest in central region of the bottom surface.

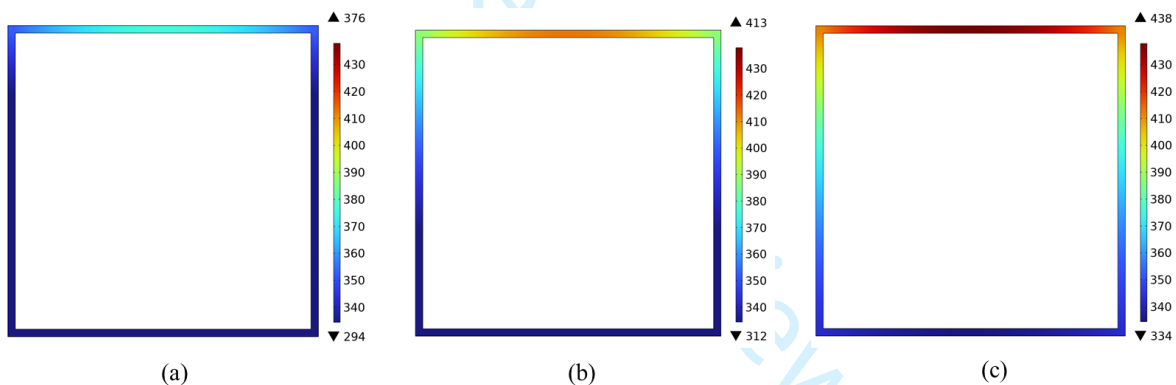


Fig. 4 Temperature distributions of the cross-section at the moment of (a) 1000s, (b) 2000s and (c) 3000s when the angle of solar radiation is 0° .

During the in-orbit operation process of spacecrafts, the occurrence of a solar eclipse often leads to a sudden change in the heating source, significantly impacting the temperature fields of the structures. A numerical example is conducted to evaluate the effect of solar eclipse on the temperature field of thin-walled beams. In the numerical example, solar radiation perpendicularly loads the top surface during the interval time 0-3000s while the solar heat flux suddenly disappears at 3000s. The result, demonstrated in Figure 6, shows that the temperature on the sunny side (top surface) continuously decreases when the eclipse happens. However, the temperature of shaded side (bottom surface) steadily increases until 4000 s, where it reaches a maximum. Subsequently, it starts to drop until

the temperature at top and bottom surfaces equals may be explained by the huge temperature difference along the z -direction.

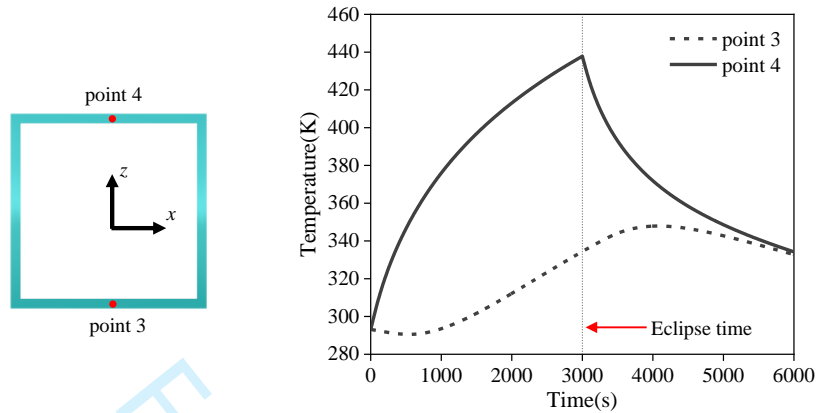


Fig. 5 Time history distributions of temperature of two points with coordinate of $x=0$, $z=-50\text{mm}$ and $x=0$, $z=50\text{mm}$ when solar eclipse occurs at the moment of 3000s.

For the purpose of examining the influence of the angle of solar radiation on the temperature distribution of thin-walled beams, several numerical examples with varying angles of heating sources are carried out. Figure 7 shows the two-dimensional temperature distribution on the cross-section at the heating angles $\theta=15^\circ$, $\theta=30^\circ$, $\theta=45^\circ$, respectively. The temperature distributions across the cross-section reveal a noticeable increase in both the lowest and highest temperatures as the angle increase from 15° to 45° . Figure 8 illustrates the temperature distributions along three red lines shown in (a), (b) and (c). When the angle increases from 15° to 30° and 45° , temperature gradient of the left edge along z -direction continuously decreases, as depicted in Figure 8 (a). Figure 8 (b) displays the temperature distribution of the bottom edge along x -direction, highlighting a substantial temperature increase at all points as the angle shifts from 15° to 30° and 45° . Lastly, for the top edge, the temperature gradient at 45° is significantly higher compared to 15° and 30° .

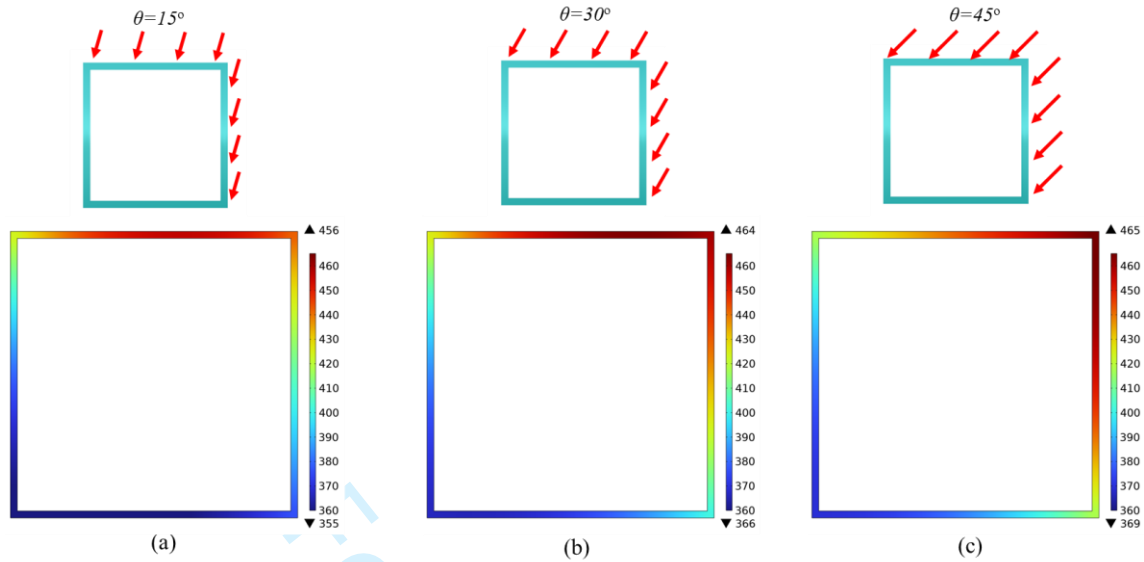


Fig. 6 Temperature distributions of the cross-section at the moment of 3000s when the angle of solar radiation θ is (a) 15° , (b) 30° , (c) 45° .

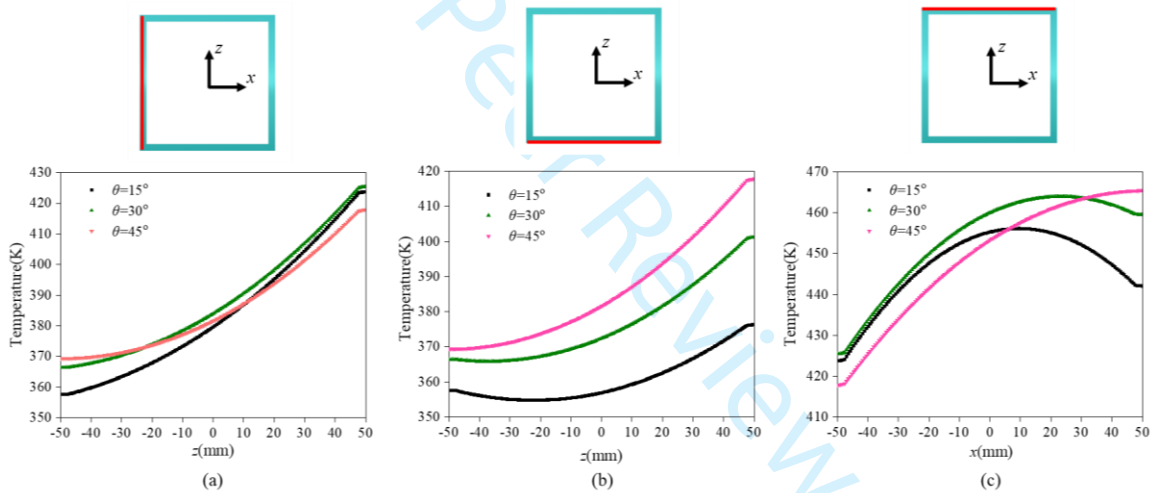


Fig. 7 Temperature distributions of (a) left edge along z -direction, (b) bottom edge along x -direction and (c) top edge along x -direction under different angle of solar heating.

C. Effect of local shadows on temperature distributions

The numerical examples discussed above have exclusively taken into account a constant heat flux along the axis direction. However, thin-walled beams may encounter shadows cast by other structural components of the aerospace crafts. The shadow effect, which is also considered in the present method, has a strong impact on the temperature field of thin-walled beams. Therefore, a thin-walled beam under solar heat flux with a shadow area on the right top edge is shown in Figure 9 (a). The length of shadow area is $L_s=3.0\text{m}$, which is assumed to be independent from the time history. When the solar heat flux becomes variable along the axis direction, the discretization of the

longitudinal direction probably assumes a strong impact on the thermal result. For the sake of determining the most suitable model, several types of discretization models using B2 or B4 element are established to compute the temperature results, as depicted in Figure 9 (b) and (c). The specifics of each type of discretization are described as follows. The length of every element is 1m for the 6B2 type, 0.5m for the 12B2 type and, 0.25m for the 24B2 type. The 3B4 model owns one 2.25m length B4 element, one 0.75m length B4 element in the middle area and one 3m length B4 element. The 8B4 type owns eight 0.75m B4 elements. A FEM model using linear hexahedral element with a total DOFs number of 200080 is established for the validation of the CUF results. Observing Figure 9 (b) and (c), it is evident that the CUF results get progressively closer to the FEM results as the total number of beam element nodes increases. The comparison between the 8B4 and 24B2 models reveals that the B4 element is better suited for addressing the shadow problem. In the 24B2 result, there is still a noticeable fluctuation, as indicated by the blue dotted line in Figure 9 (b) and (c). Hence, the 8B4 element discretization is applied in the following numerical examples with consideration of the shadow effect.

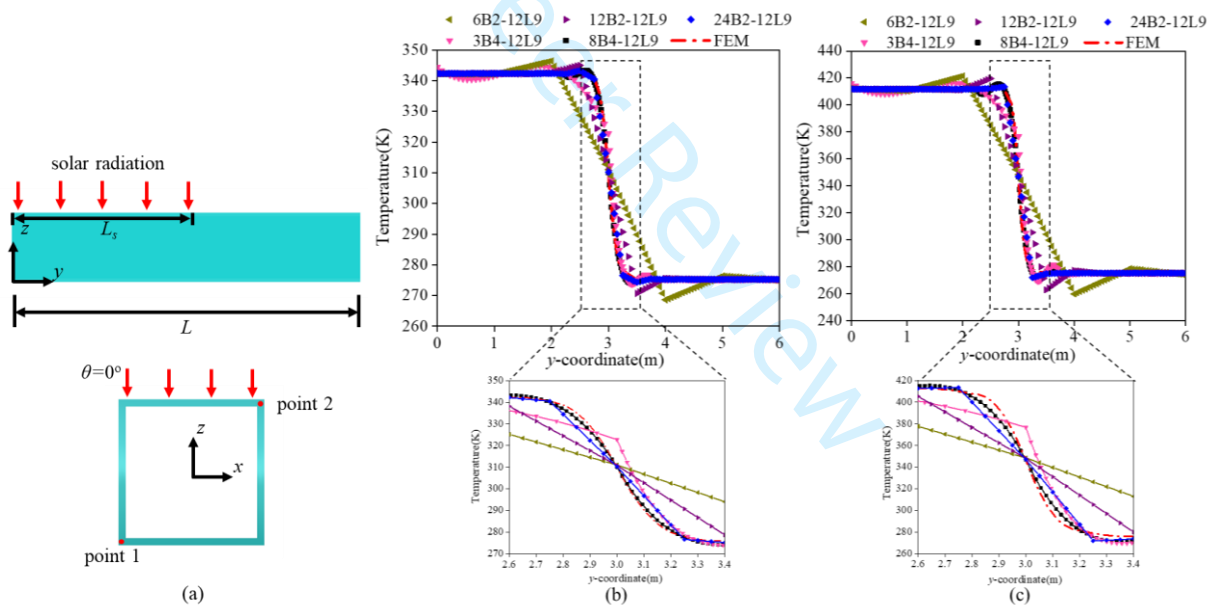


Fig. 8 (a) Schematic diagram of a thin-walled beam under solar heating which is partially sheltered; (b) (c) temperature distributions along the y -direction of point 1 and point 2 using different discretization models.

Figure 10 (b) and (c) demonstrate the temperature distributions along axis direction of two different points under 0° , 15° , 30° and 45° angles of solar radiation $t=3000s$. The locations of two points on cross-section are shown in Figure 10 (a). At point 1, it is found a significant temperature increment as the angle continuously increases within the solar radiation range. On the contrary, no evident changes occur increasing the angle within the shadow area. A similar phenomenon can be discovered at point 2 in Figure 10 (c).

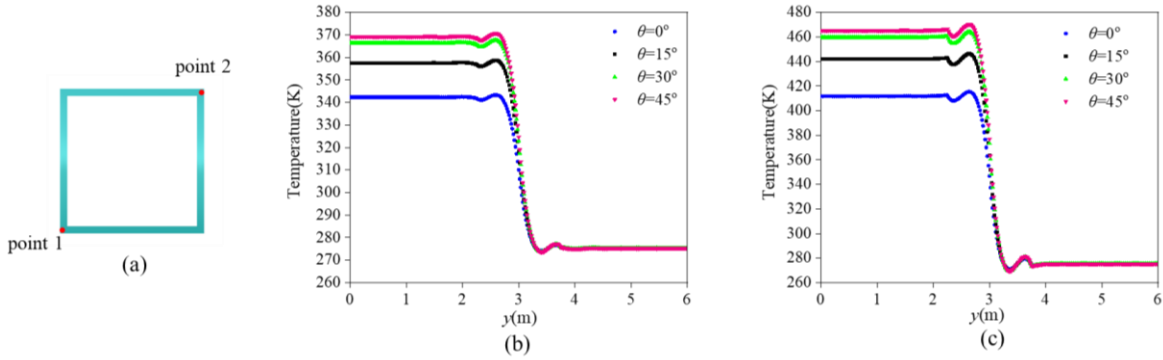
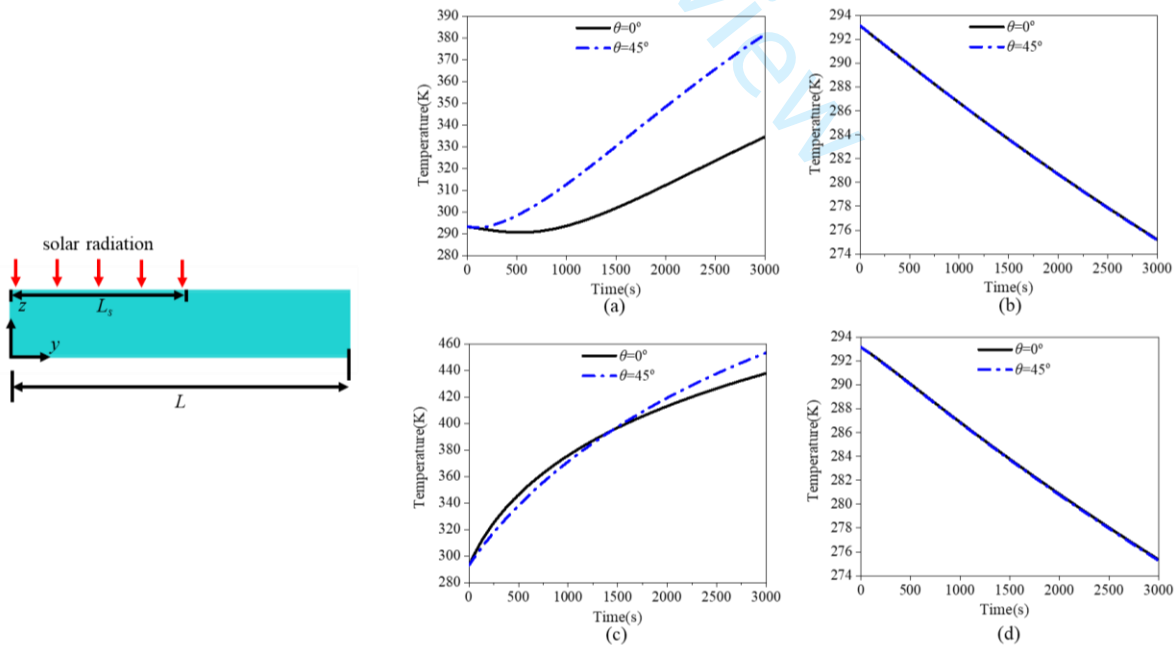


Fig. 9 (a) Locations of point 1 and 2; temperature distributions of (b) point 1 and (c) point 2 along y-direction when angles of solar radiation are 0°, 15°, 30° and 45°, respectively.

Figure 11 (a)-(d) exhibit the time history distributions of temperature of four different points with coordinates of $x=0$ $y=1500$ mm $z=-50$ mm, $x=0$ $y=4500$ mm $z=-50$ mm, $x=0$ $y=1500$ mm $z=50$ mm, $x=0$ $y=4500$ mm $z=50$ mm, under the same heating source of Figure 9 and 10. Clearly, the first and third points are located in the solar radiation area, whereas the second and fourth points are located in the shaded area. The results in Figure 11 (a) and (c) reveal that variation tendency of temperature is similar to the situation depicted in Figure 4. Nevertheless, for the points located in shaded areas, the constant temperature decrease suggests that the effect of radiation dissipation is more remarkable. On the other hand, for the points located in solar area, the incident angle of solar radiation has a significant influence on the time history distributions of temperature. The influence is negligible for the points located in shaded area.



1
2
3 **Fig. 10 Time history distributions of temperature of (a) $x=0$ $y=1500\text{mm}$ $z=-50\text{mm}$, (b) $x=0$ $y=4500\text{mm}$ $z=-$**
4 **50mm , (c) $x=0$ $y=1500\text{mm}$ $z=50\text{mm}$ and $x=0$ $y=4500\text{mm}$ $z=50\text{mm}$ when angles of solar radiation are 0° and**
5 **45° , respectively.**
6

7 **V. Conclusion**

8
9 In the present paper, a novel approach in the framework of CUF theory is proposed for solving transient thermal
10 problems of thin-walled structures in outer space. The governing equations of the temperature field is established by
11 introducing the weight residual method. To solve the equations, temperature fields of cross-section are described as
12 through Lagrange polynomials, which are also known as LE model. Linear beam element (B2) and third-order beam
13 element (B4) are involved in the discretization along the longitudinal direction. Given the initial temperature
14 condition, the nonlinear ODEs can be calculated using the numerical Adams-Bashforth method. In the numerical
15 examples, convergence analyses of the temperature results reveal that the accuracy of L9 expansion is significantly
16 higher than L4 expansion. Finally, the paper discusses the effect of several factors including solar radiation angles,
17 shadow impact on temperature distribution along different directions and time. The present work introduces a
18 method with superior computational efficiency and accuracy compared to traditional FEM for obtaining transient
19 temperature fields of space thin-walled structures.
20
21
22
23
24
25
26
27
28
29
30

31 **Funding Sources**

32
33 The authors acknowledge the supports from the Key Scientific and Technological Projects of Henan Province
34 of China (No. 222102210263).
35
36
37

38 **References**

- 39
40
41 [1] Gulick D W, Thornton E A. "Thermally-induced vibrations of a spinning spacecraft boom," *Acta Astronautica*, Vol. 36, No.
42 3, 1995, pp. 163-176.
43 [https://doi.org/10.1016/0094-5765\(95\)00097-J](https://doi.org/10.1016/0094-5765(95)00097-J)
44
45 [2] Cao Y. T., Cao D. Q., He G. Q., Liu L., "Thermal Alternation Induced Vibration Analysis of Spacecraft with Lateral Solar
46 Arrays in Orbit," *Applied Mathematical Modelling*, Vol. 86, 2020, pp. 166-184.
47 <https://doi.org/10.1016/j.apm.2020.05.008>
48
49 [3] Tran T. Q. N., Lee H. P., Lim S. P., "Structural intensity analysis of thin laminated composite plates subjected to thermally
50 induced vibration," *Composite Structures*, Vol. 78, No. 1, 2007, pp. 70-83.
51 <https://doi.org/10.1016/j.compstruct.2005.08.019>
52
53
54
55
56
57
58
59
60

- 1
2
3 [4] E. Carrera, A. Varello, "Dynamic response of thin-walled structures by variable kinematic one-dimensional models," *Journal*
4 *of Sound & Vibration*, Vol. 331, No. 24, 2012, pp. 5268-5282.
5
6 <http://dx.doi.org/10.1016/j.jsv.2012.07.006>
7
8 [5] Johnston J. D., Thornton E. A., "Thermally Induced Attitude Dynamics of a Spacecraft with a Flexible Appendage," *Journal*
9 *of Guidance Control & Dynamics*, Vol.21, No. 4, 1998, pp. 581-587.
10
11 <https://doi.org/10.2514/2.4297>
12
13 [6] Yang H., Daneshkhah E., Xu X., "Numerical vibration correlation technique for thin-walled composite beams under
14 compression based on accurate refined finite element," *Composite structures*, Vol. 280, 2022, 114861.
15
16 <https://doi.org/10.1016/j.compstruct.2021.114861>
17
18 [7] Murozono M., Ea. T., "Buckling and quasistatic thermal-structural response of asymmetric rolled-up solar array," *Journal of*
19 *spacecraft and rockets*, Vol.35, 1998, pp. 147-155.
20
21 <https://doi.org/10.2514/2.3322>
22
23 [8] Johnston J. D., Thornton E. A., "Thermal response of radiantly heated spinning spacecraft booms," *Journal of Thermophysics*
24 *and Heat Transfer*, Vol. 10, 1996, pp. 60-68.
25
26 <https://doi.org/10.2514/3.753>
27
28 [9] Lu Q. Y., Rizwan-uddin, "A finite element approach for nonlinear, transient heat conduction problems with convection,
29 radiation or contact boundary conditions," *Annals of Nuclear Energy*, Vol. 193, 2023, 110009.
30
31 <https://doi.org/10.1016/j.anucene.2023.110009>
32
33 [10] Wang B. L., Mai Y. W., "Transient one-dimensional heat conduction problems solved by finite element," *International*
34 *Journal of Mechanical Sciences*, Vol. 47, No. 2, 2005, pp. 303-317.
35
36 <https://doi.org/10.1016/j.ijmecsci.2004.11.001>
37
38 [11] Shen Z. X., Hao S. W., Li H. J., "Comparison of various thin-walled composite beam models for thermally induced
39 vibrations of spacecraft boom," *Composite Structures*, Vol. 320, 2023, 117163.
40
41 <https://doi.org/10.1016/j.compstruct.2023.117163>
42
43 [12] Lutz J. D., Allen D. H., Haisler W. E., "Finite-element model for the thermoelastic analysis of large composite space
44 structures," *Journal of Spacecraft & Rockets*, Vol. 24, No. 5, 1987, pp. 430-436.
45
46 <https://doi.org/10.2514/3.25935>
47
48 [13] Thornton E. A., Kim Y. A., "Thermally induced bending vibrations of a flexible rolled-up solar array," *Journal of*
49 *Spacecraft and Rockets*, Vol.30, No. 4, 1993, pp. 438-448.
50
51 <https://doi.org/10.2514/3.25550>
52
53
54
55
56
57
58
59
60

- 1
2
3 [14] Johnston J. D., Thornton E. A., "Thermally Induced Dynamics of Satellite Solar Panels," *Journal of Spacecraft & Rockets*,
4 Vol.37, No.5, 2000, pp. 604-613.
5
6 <https://doi.org/10.2514/2.3633>
7
8 [15] Ding Y., Xue M. D., "Transient Thermal-Structural Analysis of Space Structures Consisting of Thin-Walled Tubes by
9 FEM," *Chinese Journal of Applied Mechanics*, Vol. 20, No.1, 2003, pp. 42-48.
10
11 [16] Xue M. D., Ding Y., "Two kinds of tube elements for transient thermal-structural analysis of large space structures,"
12 *International Journal for Numerical Methods in Engineering*, Vol. 59, No. 10, 2004, pp. 1335-1353.
13
14 <https://doi.org/10.1002/nme.918>
15
16 [17] Ding Y., Xue M.D., Kim J. K., "Thermo-structural analysis of space structures using Fourier tube elements," *Computational*
17 *Mechanics*, Vol. 36, No. 4, 2005, pp. 289-297.
18
19 <https://doi.org/10.1007/s00466-005-0666-5>
20
21 [18] Xue M. D., Duan J., Xiang Z. H., "Thermally-induced bending-torsion coupling vibration of large-scale space structures,"
22 *Computational Mechanics*, Vol. 40, No. 4, 2007, pp. 707-723.
23
24 <https://doi.org/10.1007/s00466-006-0134-x>
25
26 [19] Li W., Xiang Z. H., Cheng L. J., Xue M. D., "Thermal flutter analysis of large-scale space structures based on finite element
27 method," *International Journal for Numerical Methods in Engineering*, Vol. 69, No. 5, 2007, pp. 887-907.
28
29 <https://doi.org/10.1002/nme.1793>
30
31 [20] Duan J., Xiang Z. H., Xue M. D., "Thermal-dynamic coupling analysis of large space structures considering geometric
32 nonlinearity," *International Journal of Structural Stability and Dynamics*, Vol. 8, No. 4, 2008, pp. 569-596.
33
34 <https://doi.org/10.1142/S0219455408002806>
35
36 [21] E. Carrera, M. Cinefra, M. Petrolo, E. Zappino, *Finite Element Analysis of Structures Through Unified Formulation*. John
37 Wiley & Sons, Inc, 2014.
38
39 <https://onlinelibrary.wiley.com/doi/book/10.1002/9781118536643>
40
41 [22] A. Pagani, M. Petrolo, G. Colonna, E. Carrera, "Dynamic response of aerospace structures by means of refined beam
42 theories," *Aerospace Science and Technology*, Vol. 46, 2015, pp. 360-373.
43
44 <https://doi.org/10.1016/j.ast.2015.08.005>
45
46 [23] Bharati R. B., Fillipi M., Mahato P. K., E. Carrera, "Flutter analysis of laminated composite structures using Carrera Unified
47 Formulation," *Composite Structures*, Vol. 253, 2020, 112759.
48
49 <https://doi.org/10.1016/j.compstruct.2020.112759>
50
51 [24] B. Wu, A. Pagani, M. Filippi, W. Q. Chen, E. Carrera, "Accurate stress fields of post-buckled laminated composite beams
52 accounting for various kinematics," *International Journal of Non-Linear Mechanics*, Vol. 111, 2019, pp. 60-71.
53
54
55
56
57
58
59
60

1
2
3 <https://doi.org/10.1016/j.ijnonlinmec.2019.02.002>

4 [25] M. Afzali, M. Farrokh, E. Carrera, “Thermal buckling loads of rectangular FG plates with temperature-dependent properties
5 using Carrera Unified Formulation,” *Composite structures*, Vol. 295, 2022, 115787.

6
7 <https://doi.org/10.1016/j.compstruct.2022.115787>

8 [26] Y. Yan, A. Pagani, E. Carrera, “Thermal buckling solutions of generic metallic and laminated structures: Total and updated
9 Lagrangian formulations via refined beam elements,” *Journal of Thermal Stresses*, Vol. 45, No. 8, 2022, pp. 669–694.

10
11 <https://doi.org/10.1080/01495739.2022.2090471>

12 [27] E. Carrera, A. Pagani, R. Augello, “Large deflection of composite beams by finite elements with node-dependent
13 kinematics,” *Computational Mechanics*, Vol. 69, No. 6, 2022, pp. 1481–1500.

14
15 <https://doi.org/10.1007/s00466-022-02151-4>

16 [28] E. Carrera, A. Pagani, “Free vibration analysis of civil engineering structures by component-wise models,” *Journal of Sound
17 and Vibration*, Vol. 333, No. 19, 2014, pp. 4597–4620.

18
19 <https://doi.org/10.1016/j.jsv.2014.04.063>

20 [29] R. Augello, E. Daneshkhah, X. Xu, E. Carrera, “Efficient CUF-based method for the vibrations of thin-walled open cross-
21 section beams under compression,” *Journal of Sound and Vibration*, Vol. 510, 2021, pp. 116232.

22
23 <https://doi.org/10.1016/j.jsv.2021.116232>

24 [30] F. Miglioretti, E. Carrera, “Application of a Refined Multi-Field Beam Model for the Analysis of Complex Configurations,”
25 *Mechanics of Advanced Materials and Structures*, Vol. 22, No. 1-2, 2015, pp. 52-66.

26
27 <https://doi.org/10.1080/15376494.2014.912365>

28 [31] X. Y. Xu, E. Carrera, R. Augello, E. Daneshkhah, H. Yang, “Benchmarks for higher-order modes evaluation in the free
29 vibration response of open thin-walled beams due to the cross-sectional deformations,” *Thin-Walled Structures*, Vol. 166,
30 2021, 107965.

31
32 <https://doi.org/10.1016/j.tws.2021.107965>

33 [32] A. Pagani, R. Augello, E. Carrera, “Frequency and mode change in the large deflection and post-buckling of compact and
34 thin-walled beams,” *Journal of Sound & Vibration*, Vol. 432, 2018, pp. 88-104.

35
36 <https://doi.org/10.1016/j.jsv.2018.06.024>

37 [33] E. Carrera, F. A. Fazzolari, M. Cinefra, *Thermal Stress Analysis of Composite Beams, Plates and Shells: Computational
38 Modelling and Applications*, Academic Press, 2016.

39 [34] E. Carrera, G. Giunta, M. Petrolo, *Beam Structures: Classical and Advanced Theories*, John Wiley & Sons, 2011.